Computers and Structures 129 (2013) 178–193

Contents lists available at SciVerse ScienceDirect

Computers and Structures

journal homepage: www.elsevier.com/locate/compstruc

An explicit time integration scheme for the analysis of wave propagations

Gunwoo Noh, Klaus-Jürgen Bathe *

Massachusetts Institute of Technology, Cambridge, MA 02139, United States

ARTICLE INFO

Article history:
Received 24 April 2013
Accepted 18 June 2013
Available online 3 August 2013

Keywords:
Wave propagation
Finite elements
Explicit time integration
Desirable numerical dissipation
Numerical dispersion
Bathe implicit time integration

ABSTRACT

A new explicit time integration scheme is presented for the solution of wave propagation problems. The method is designed to have small solution errors in the frequency range that can spatially be represented and to cut out high spurious frequencies. The proposed explicit scheme is second-order accurate for systems with and without damping, even when used with a non-diagonal damping matrix. The stability, accuracy and numerical dispersion are analyzed, and solutions to problems are given that illustrate the performance of the scheme.

1. Introduction

Direct time integration is widely used in finite element solutions of structural dynamics and transient wave propagation problems, and schemes can be categorized into two groups: explicit and implicit methods. A time integration method is implicit if the solution procedure requires the factorization of an 'effective stiffness' matrix and is explicit otherwise [1–3].

In general, each type of integration has its own advantages and disadvantages. Implicit methods require a much larger computational effort per time step when compared with explicit methods. However, implicit methods can be designed to have unconditional stability, in linear analysis, so that the time step size can be selected solely based on the characteristics of the problem to be solved. On the other hand, explicit methods when using a diagonal mass matrix may require only vector calculations. Hence, the computational cost per time step is much lower. However, an explicit method can only be conditionally stable. Therefore, explicit methods may be effective when the time step size required by the stability limit is about the same as the time step size needed to describe the physical problem, and this is frequently the case in wave propagation analyses [1–6].

Accurate finite element solutions of wave propagations are difficult to obtain. Numerical errors due to the spatial and time discretizations resulting in artificial period elongations and amplitude decays, seen as numerical dispersions and dissipations, often render finite element solutions of wave propagation problems to be quite inaccurate [1,6–10]. In particular, large errors in just the few highest frequency modes contained in the mesh shown as spurious oscillations can severely impair the accuracy of the solution. These spurious oscillations may increase in time since the dispersion and dissipation errors accumulate as the waves propagate.

Much research effort, following different approaches, has been focused on reducing the dispersion and dissipation errors. Of course, to reduce the errors from the spatial discretization, higher-order spatial discretizations can be employed [11–16]. However, the use of high-order elements can be computationally expensive and may not have the generality as does the use of the traditional finite element procedures employing low-order elements. Linear combinations of consistent and lumped mass matrices [17–21] or modified spatial integration rules for evaluations of mass and stiffness matrices [22–24] may also be used to obtain better solution accuracy. However, these schemes are different from those commonly used in structural dynamics and do not lead to a general solution procedure. Errors due to the spurious oscillations can also be reduced by the use of filtering [24–26] for specific points in space and time. These schemes can be valuable to obtain improved solutions for a number of spatial and time points but in engineering practice, accurate solutions are generally sought over the complete problem geometry and all time considered.

Many direct time integration schemes introduce numerical dissipation to improve the solution by suppressing the high frequency spurious modes [1,2,27,28]. However, it is difficult to obtain an effective scheme, since the numerical dissipation should be large

* Corresponding author. Tel.: +1 6179265199.
E-mail address: kjb@mit.edu (K.J. Bathe).

0045-7949/$ - see front matter © 2013 Elsevier Ltd. All rights reserved.
http://dx.doi.org/10.1016/j.compstruc.2013.06.007

enough to suppress the high frequency spurious modes, while at the same time keeping good accuracy in the low frequency modes. The search for an effective such scheme is very important since, in engineering practice, such method could be used for structural dynamics and wave propagation problems in a uniform manner.

Among implicit methods, the Bathe method [29–31] has been shown to result in remarkably accurate solutions by suppressing the high frequency spurious modes [6]. The property of this scheme to 'cut out' high frequency modes that cannot be spatially resolved and to integrate those modes accurately that can be spatially resolved results into relatively small dispersion error [6,32].

Considering explicit methods, the central difference method is still a widely used scheme. It has the largest time step stability limit of any second-order accurate explicit method [33,34]. However, the central difference method requires a matrix factorization for systems with a non-diagonal damping matrix, a shortcoming that has been addressed, see e.g. Refs. [35,36], and in particular, since the method is a non-dissipative scheme, the solution accuracy can be severely ruined by the dispersion errors in the high frequency modes.

The development of dissipative explicit methods has been much pursued [37]. Schemes have been presented by Newmark [38],

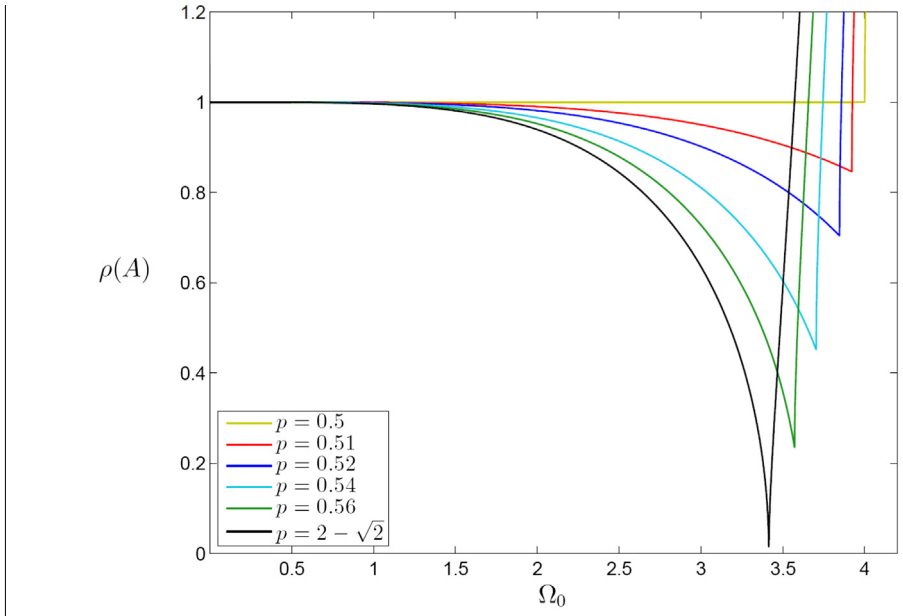

(a) Spectral radii of approximation operator when $\xi = 0$

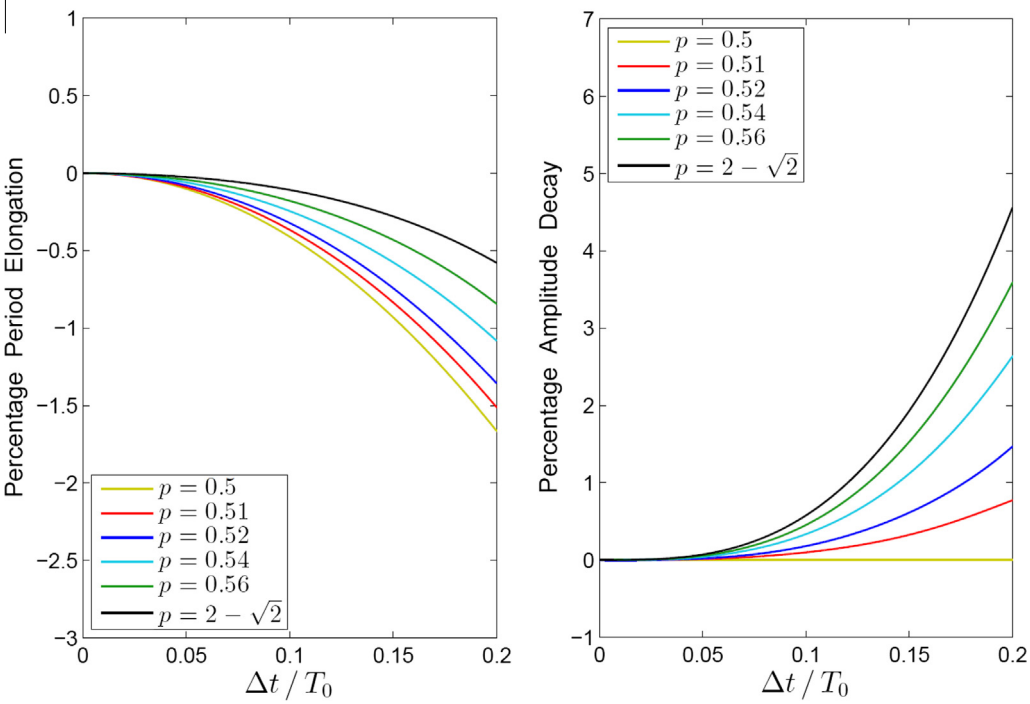

(b) Percentage period elongations and amplitude decays

Fig. 1. Proposed scheme for various values of p.

Chung and Lee [3], Zhai [39], Hulbert and Chung [4] and Tchamwa et al. [40]. The Newmark explicit method and the Zhai explicit scheme with high-frequency dissipation are only first order accurate and decrease the solution accuracy in the low frequency domain. The Tchamwa–Wielgosz method is also only first order accurate. Comparative studies [41,42] have shown that the remaining dissipative explicit methods are second-order accurate but often provide less accurate solutions than the Tchamwa–Wielgosz scheme.

In this paper, we present a new explicit time integration scheme for the analysis of wave propagations. We first focus on the formulation of the method and its stability and accuracy characteristics. Then we study the dispersion properties of the method using 4-node elements in two-dimensional solutions. Finally, for an evaluation, we provide the calculated response in the solution of various problems using the proposed scheme and the central difference and Tchamwa–Wielgosz methods.

2. An explicit time integration scheme

Considering linear analysis, the governing finite element equations to be solved are

$$\mathbf{M}\ddot{\mathbf{U}} + \mathbf{C}\dot{\mathbf{U}} + \mathbf{K}\mathbf{U} = \mathbf{R} \tag{1}$$

with given initial conditions, where **M**, **C**, **K** are the mass, damping and stiffness matrices and the vectors **U** and **R** list, respectively, the nodal displacements and externally applied nodal forces. An overdot denotes a time derivative. If the time step size Δt is set and all primary solution variables are known up to time t, then the time integration scheme is to calculate the solution at time $t + \Delta t$.

The approach used in the proposed explicit scheme is to calculate the unknown displacements, velocities and accelerations by considering the time step Δt to consist of two sub-steps, as inspired by the Bathe implicit method. The time step sizes are $p\Delta t$ and $(1-p)\Delta t$ for the first and the second sub-step, respectively, where $p \in (0,1)$.

We consider, in the first sub-step,

$$\mathbf{M}\,{}^{t+p\Delta t}\ddot{\mathbf{U}} + \mathbf{C}\,{}^{t+p\Delta t}\tilde{\dot{\mathbf{U}}} + \mathbf{K}\,{}^{t+p\Delta t}\mathbf{U} = {}^{t+p\Delta t}\hat{\mathbf{R}} \tag{2}$$

$${}^{t+p\Delta t}\mathbf{U} = {}^{t}\mathbf{U} + [p\Delta t]\,{}^{t}\dot{\mathbf{U}} + \frac{1}{2}[p\Delta t]^2\,{}^{t}\ddot{\mathbf{U}} \tag{3}$$

$${}^{t+p\Delta t}\hat{\dot{\mathbf{U}}} = {}^{t}\dot{\mathbf{U}} + \frac{1}{2}[p\Delta t]\,{}^{t}\ddot{\mathbf{U}} \tag{4}$$

$${}^{t+p\Delta t}\dot{\mathbf{U}} = {}^{t+p\Delta t}\hat{\dot{\mathbf{U}}} + \frac{1}{2}[p\Delta t]\,{}^{t+p\Delta t}\ddot{\mathbf{U}} \tag{5}$$

and in the second sub-step,

$$\mathbf{M}\,{}^{t+\Delta t}\ddot{\mathbf{U}} + \mathbf{C}\,{}^{t+\Delta t}\tilde{\dot{\mathbf{U}}} + \mathbf{K}\,{}^{t+\Delta t}\mathbf{U} = {}^{t+\Delta t}\mathbf{R} \tag{6}$$

$${}^{t+\Delta t}\mathbf{U} = {}^{t+p\Delta t}\mathbf{U} + [(1-p)\Delta t]\,{}^{t+p\Delta t}\dot{\mathbf{U}} + \frac{1}{2}[(1-p)\Delta t]^2\,{}^{t+p\Delta t}\ddot{\mathbf{U}} \tag{7}$$

$${}^{t+\Delta t}\hat{\dot{\mathbf{U}}} = {}^{t+p\Delta t}\dot{\mathbf{U}} + \frac{1}{2}[(1-p)\Delta t]\,{}^{t+p\Delta t}\ddot{\mathbf{U}} \tag{8}$$

$${}^{t+\Delta t}\dot{\mathbf{U}} = {}^{t+\Delta t}\hat{\dot{\mathbf{U}}} + [(1-p)\Delta t]\left(q_0\,{}^{t}\ddot{\mathbf{U}} + q_1\,{}^{t+p\Delta t}\ddot{\mathbf{U}} + q_2\,{}^{t+\Delta t}\ddot{\mathbf{U}}\right) \tag{9}$$

where in the following equations we use Eqs. (4) and (8)

$${}^{t+p\Delta t}\tilde{\dot{\mathbf{U}}} = (1-s)\,{}^{t+p\Delta t}\hat{\dot{\mathbf{U}}} + s\,{}^{t}\dot{\mathbf{U}} \tag{10}$$

$${}^{t+\Delta t}\tilde{\dot{\mathbf{U}}} = (1-s)\,{}^{t+\Delta t}\hat{\dot{\mathbf{U}}} + s\,{}^{t+p\Delta t}\dot{\mathbf{U}} \tag{11}$$

and p, q_0, q_1, q_2 and s are parameters to be determined. These parameters, of course, affect the stability and accuracy characteristics of the method. Which load best to use at the sub-step, ${}^{t+p\Delta t}\hat{\mathbf{R}}$, is addressed in Section 2.3. We may interpret the first sub-step as using a finite difference Euler forward step followed by using the trapezoidal rule for the final velocities (like in the central difference method, involving only the velocities at the beginning of the sub-step and the accelerations at the beginning and at the end of the sub-step). The second sub-step can be seen as the same predictor–corrector but with an equation for the final velocities using the three accelerations involved in the step. The proposed form is inherently explicit with a lumped mass matrix and any damping matrix. Of course, the $\mathbf{K}\,{}^{t+p\Delta t}\mathbf{U}$ and $\mathbf{K}\,{}^{t+\Delta t}\mathbf{U}$ terms could be evaluated without calculating stiffness matrices but summing over element force vectors [1], and the same holds for the damping matrix terms.

2.1. Stability and accuracy characteristics

To have second order accuracy, we use, with and without physical damping included,

$$q_0 + q_1 + q_2 = \frac{1}{2}; \quad q_2 = \frac{1}{2} - pq_1; \quad s = -1 \tag{12}$$

Here, actually, $s = -1$ is not required when **C** is not included, which is clear from Eqs. (2) and (6).

In the decoupled modal equations, the method may be expressed as [1]

$$\begin{bmatrix} {}^{t+\Delta t}\ddot{x} \\ {}^{t+\Delta t}\dot{x} \\ {}^{t+\Delta t}x \end{bmatrix} = \mathbf{A}\begin{bmatrix} {}^{t}\ddot{x} \\ {}^{t}\dot{x} \\ {}^{t}x \end{bmatrix} + \mathbf{L_a}\,{}^{t+p\Delta t}r + \mathbf{L_b}\,{}^{t+\Delta t}r \tag{13}$$

where **A**, $\mathbf{L_a}$ and $\mathbf{L_b}$ are the integration approximation and load operators, respectively. The stability and some accuracy characteristics of the method may be studied using this form of the scheme.

Using the relations in Eq. (12) and considering the case of no physical damping, the characteristic polynomial of **A** becomes

$$\tilde{p}(\lambda) = \lambda^3 - 2A_1\lambda^2 + A_2\lambda - A_3 \tag{14}$$

where

$$\begin{aligned} A_1 &= 1 - \frac{1}{2}\omega_0^2\Delta t^2 + \frac{1}{4}p(1-p)\left(p^2q_1 - pq_1 + \frac{1}{2}\right)\omega_0^4\Delta t^4; \\ A_2 &= 1 + \frac{1}{2}pq_1(1-p)^3\omega_0^4\Delta t^4; \\ A_3 &= 0 \end{aligned} \tag{15}$$

and ω_0 is the modal natural frequency. Using the Routh–Hurwitz stability criteria on Eq. (14), and $\Omega_0 = \omega_0\Delta t$ we obtain the expression for the maximum stability limit

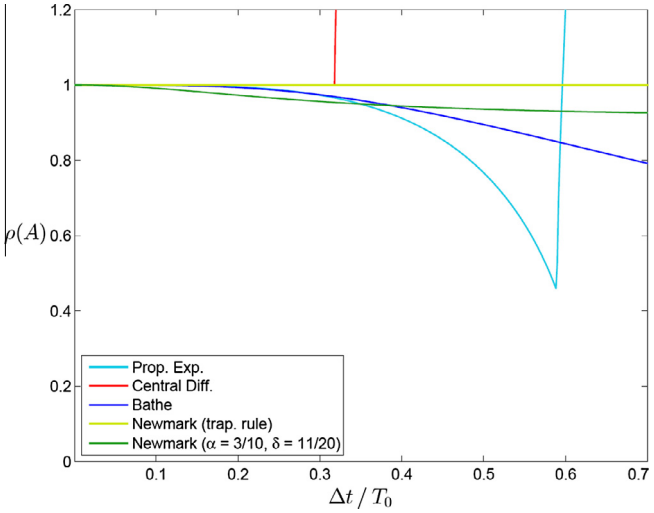

Fig. 2. Spectral radii of approximation operators, case $\xi = 0$, for various methods; for the proposed explicit scheme, $p = 0.54$ is used.

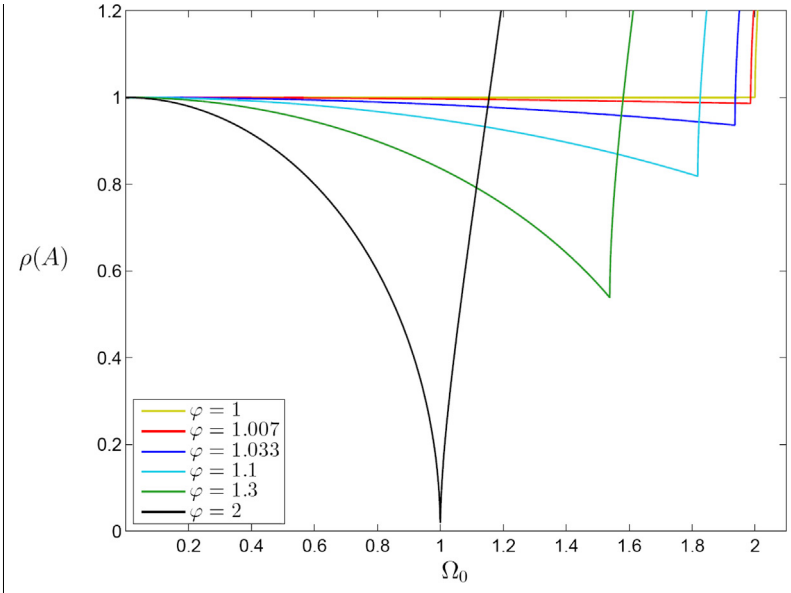

(a) Spectral radii of approximation operator when $\xi = 0$

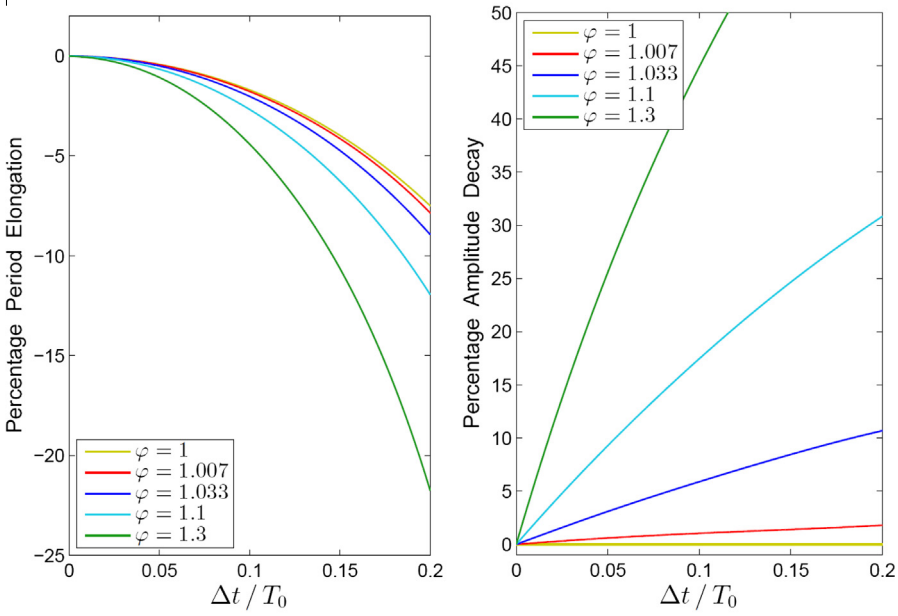

(b) Percentage period elongations and amplitude decays

Fig. 3. Tchamwa–Wielgosz scheme for various values of φ.

$$\Omega_s^2 = \frac{1}{\gamma p(1-p)} \tag{16}$$

with the conditions

$$-\frac{1}{4(1-p)} \leqslant q_1 \leqslant \frac{4p(1-p)-1}{8(1-p)^2 p}; \quad \gamma = \frac{1}{4} - \frac{1}{2}(1-p)q_1 \tag{17}$$

where $\Omega_s = \omega_0 \Delta t_{cr}$ and Δt_{cr} is the critical time step. Hence if $p = 0.5$ and $q_1 = 0$, the stability limit $\Omega_s = 4$ and the method has the stability limit twice that of the central difference method but uses the substep; see Section 2.3 for a remark regarding the computational expense in using the method.

To represent oscillatory solutions, the eigenvalues of **A** should remain in the complex plane. Since $A_3 = 0$, we have a zero eigenvalue and

$$\lambda_{1,2} = A_1 \pm \sqrt{A_1^2 - A_2} \tag{18}$$

The bifurcation points where the eigenvalues become real, are given by

$$\Omega_{b1}^2 = \frac{2}{\alpha(1-p)}; \quad \Omega_{b2,3}^2 = \frac{2 - p \pm \sqrt{\beta}}{\alpha(1-p)p} \tag{19}$$

with

$$\alpha = \frac{1}{2} - (1-p)pq_1; \quad \beta = 8p(p-1)^2 q_1 + p^2 \tag{20}$$

From Eq. (17), $\alpha > 0$; hence we always have a positive real bifurcation point given by Ω_{b1}. To maximize the available frequency domain, we require Ω_{b1} to be smaller so that the effective

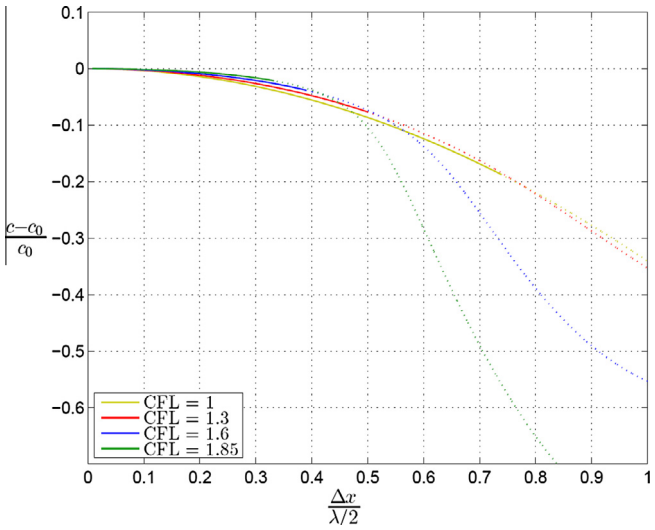

Fig. 4. Relative wave speed errors of the proposed method for various CFL numbers; using $p = 0.54$; results for discarded wave modes are given by dotted lines.

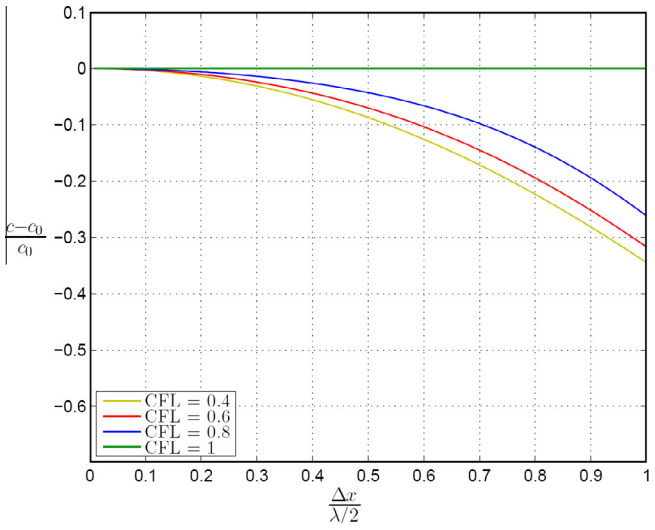

Fig. 5. Relative wave speed errors of the central difference method for various CFL numbers.

bifurcation point becomes the larger value of $\Omega_{b2,3}$ with the condition $\beta > 0$. This constraint results in

$$q_1 = \frac{1-2p}{2p(1-p)} \tag{21}$$

With Eq. (21), the bifurcation point and the stability limit are maximized as

$$\Omega_b = \frac{2}{p}; \quad \Omega_s = \frac{2}{\sqrt{(1-p)(3p-1)}} \tag{22}$$

where $1/2 \leqslant p < 2/3$ is the required condition, so that always $\Omega_b \leqslant \Omega_s$. With Eqs. (12) and (21), the operators $\mathbf{A}$, $\mathbf{L_a}$ and $\mathbf{L_b}$ are given as a function of p in Appendix A and an analysis shows that the scheme is second-order accurate. This is not surprising since the scheme is, in essence, the central difference method slightly perturbed to introduce numerical damping (we recommend below to use $p = 0.54$, that is, a value slightly larger than 0.5).

Using the spectral radius $\rho(\mathbf{A})$ at the bifurcation point, which is denoted as ρ_b, we have

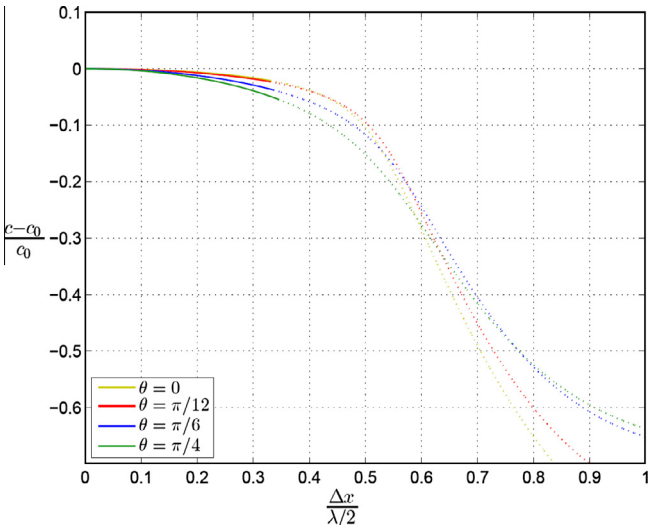

Fig. 6. Relative wave speed errors of the proposed method for various propagating angles, using CFL = 1.85 and $p = 0.54$; results for discarded wave modes are shown by dotted lines.

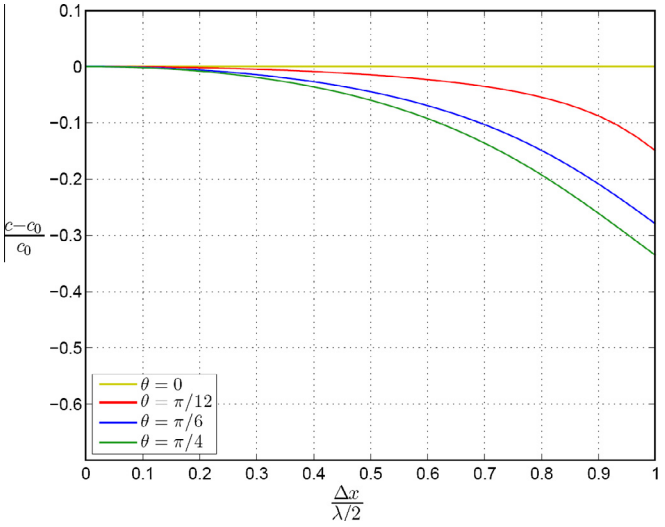

Fig. 7. Relative wave speed errors of the central difference method for various propagating angles, using CFL = 1.

$$p = \frac{2-\sqrt{2+2\rho_b}}{1-\rho_b}; \quad p = 0.5 \quad \text{if } \rho_b = 1 \tag{23}$$

Hence we may determine the value of p based on ρ_b which represents the amount of numerical dissipation in the high frequencies. The proposed method can be treated as a one parameter (p or ρ_b) method at this point. From Eq. (23), the range of p for $0 \leqslant \rho_b \leqslant 1$ is obtained as $0.5 \leqslant p \leqslant 2-\sqrt{2}$. Here $p = 0.5$ gives $\rho_b = 1$, resulting in no numerical dissipation, and $p = 2-\sqrt{2}$ results in the maximum numerical dissipation and the minimum (negative) period elongation. It is interesting to note that in the Bathe implicit integration method, the splitting ratio γ which provides the maximum dissipation and minimum period elongation is also $2-\sqrt{2}$, and at this value also the effective stiffness matrices at the sub-step and full step are identical.

Fig. 1 shows the spectral radii of the proposed method as a function of Ω_0 for various values of p. We see that for all p, $\rho(\mathbf{A}) \cong 1$ until $\Omega_0 \cong 1.25$ ($\Delta t/T_0 \cong 0.20$). This property is desirable since it will provide high accuracy for the low frequency modes. The period elongations and amplitude decays for various values of p are also given in Fig. 1 [43–45]. The results show the good accuracy charac-

teristics of the proposed scheme, which has a very small amplitude decay and (negative) period elongation for all p.

For an explicit method, it is crucial to maintain accuracy in the integration of the lower frequencies while imposing numerical dissipation in the higher frequencies just below the stability limit. Fig. 1(a) shows that the bifurcation limit of the scheme also decreases as ρ_b decreases, since using Eq. (23) p then increases, as in other dissipative explicit methods. This may also be observed in Eqs. (22) and (23). However, the relative amount of the decrease in the proposed explicit method is quite small when compared to those of other methods. Specifically, when ρ_b changes from 1 to 0 (that is, from minimum dissipation to maximum dissipation) the bifurcation limit Ω_b of the proposed method changes from 4 to 3.414, while Ω_b of the Tchamwa–Wielgosz scheme [40] changes from 2 to 1, and Ω_b for the scheme of Hulbert and Chung [4] changes from 2 to 1.414.

While the parameter p could be used to adjust, for a specific solution, the amount of numerical damping in the high frequencies, in practice, such approach would require numerical experimentation. Instead, it is desirable to have a good value of this parameter for general use, and we suggest to set $p = 0.54$. With $p = 0.54$, the scheme shows good accuracy in the low frequency response, as seen in Fig. 1(b): the period elongation is about 1% and the amplitude decay is about 2.5% when $\Delta t/T_0 = 0.2$ or smaller. Also, it has been shown that the Bathe implicit method used with CFL = 1.0 suppresses the frequencies for which $\Delta t/T_0 > 0.3$, maintaining high accuracy in the low frequencies so that surprisingly accurate solutions are obtained [6,31]. The proposed explicit method, with $p = 0.54$ (and the CFL number = $1/p \cong 1.85$) has almost the same spectral radius as the Bathe method until $\Delta t/T_0 \cong 0.3$ and thereafter a smaller spectral radius until it bifurcates, see Fig. 2. Hence, with $p = 0.54$ and CFL = 1.85 we might obtain a similar accuracy in solution results as when using the Bathe implicit method.

To compare the proposed scheme with another explicit method also designed to eliminate spurious modes, we give in Fig. 3 the spectral radii, period elongations and amplitude decays of the Tchamwa–Wielgosz scheme, recently further proposed and studied in Ref. [37]. Here the parameter φ is used to obtain different values. Comparing the spectral radii, clearly, the data of the proposed scheme indicate a more effective behaviour, and this is in fact seen when comparing the period elongations and amplitude decays, see Figs. 1 and 3. As desired, the errors are somewhat smaller for small time steps using $p = 0.54$ in the proposed scheme than when using $\varphi = 1.033$ in the Tchamwa–Wielgosz scheme (consider the use of $\Delta t/T_0 = 0.2$ for the proposed scheme and $\Delta t/T_0 = 0.1$ for the Tchamwa–Wielgosz method). However, an important point is that the curves for the amplitude decays show for the proposed scheme the desired curvature, namely small values for small time steps and rapidly increasing values for larger time steps, but not for the Tchamwa–Wielgosz method.

Table 1
Step-by-step solution using the proposed method for linear analysis with general loading.

A. *Initial calculation*

1. Form stiffness matrix $\mathbf{K}$, lumped mass matrix $\mathbf{M}$, and damping matrix $\mathbf{C}$
2. Initialize ${}^0\mathbf{U}$, ${}^0\dot{\mathbf{U}}$ and ${}^0\ddot{\mathbf{U}}$.
3. Select time step Δt and p (=0.54) and calculate integration constants:

$$q_1 = \frac{1-2p}{2p(1-p)};\quad q_2 = \frac{1}{2} - pq_1;\quad q_0 = -q_1 - q_2 + \frac{1}{2};\quad a_0 = p\Delta t;$$
$$a_1 = \frac{1}{2}(p\Delta t)^2;\quad a_2 = \frac{a_0}{2};\quad a_3 = (1-p)\Delta t;\quad a_4 = \frac{1}{2}((1-p)\Delta t)^2;$$
$$a_5 = q_0 a_3;\quad a_6 = \left(\frac{1}{2} + q_1\right)a_3;\quad a_7 = q_2 a_3;$$

B. *For each time step:*

⟨First sub-step ⟩

1. Calculate displacements and effective loads at time $t + p\Delta t$:

$${}^{t+p\Delta t}\mathbf{U} = {}^t\mathbf{U} + a_0\,{}^t\dot{\mathbf{U}} + a_1\,{}^t\ddot{\mathbf{U}}$$
$${}^{t+p\Delta t}\widehat{\mathbf{R}} = (1-p)\,{}^t\mathbf{R} + p\,{}^{t+\Delta t}\mathbf{R}$$
$${}^{t+p\Delta t}\widehat{\mathbf{R}} = {}^{t+p\Delta t}\widehat{\mathbf{R}} - \mathbf{K}\,{}^{t+p\Delta t}\mathbf{U} - \mathbf{C}({}^t\dot{\mathbf{U}} + a_0\,{}^t\ddot{\mathbf{U}})$$

2. Solve for accelerations at time $t + p\Delta t$:

$$\mathbf{M}\,{}^{t+p\Delta t}\ddot{\mathbf{U}} = {}^{t+p\Delta t}\widehat{\mathbf{R}}$$

3. Calculate velocities at time $t + p\Delta t$:

$${}^{t+p\Delta t}\dot{\mathbf{U}} = {}^t\dot{\mathbf{U}} + a_2({}^t\ddot{\mathbf{U}} + {}^{t+p\Delta t}\ddot{\mathbf{U}})$$

⟨Second sub-step ⟩

1. Calculate displacements and effective loads at time $t + \Delta t$:

$${}^{t+\Delta t}\mathbf{U} = {}^{t+p\Delta t}\mathbf{U} + a_3\,{}^{t+p\Delta t}\dot{\mathbf{U}} + a_4\,{}^{t+p\Delta t}\ddot{\mathbf{U}}$$
$${}^{t+\Delta t}\widehat{\mathbf{R}} = {}^{t+\Delta t}\mathbf{R} - \mathbf{K}\,{}^{t+\Delta t}\mathbf{U} - \mathbf{C}({}^{t+p\Delta t}\dot{\mathbf{U}} + a_3\,{}^{t+p\Delta t}\ddot{\mathbf{U}})$$

2. Solve for accelerations at time $t + \Delta t$:

$$\mathbf{M}\,{}^{t+\Delta t}\ddot{\mathbf{U}} = {}^{t+\Delta t}\widehat{\mathbf{R}}$$

3. Calculate velocities at time $t + \Delta t$:

$${}^{t+\Delta t}\dot{\mathbf{U}} = {}^{t+p\Delta t}\dot{\mathbf{U}} + a_5\,{}^t\ddot{\mathbf{U}} + a_6\,{}^{t+p\Delta t}\ddot{\mathbf{U}} + a_7\,{}^{t+\Delta t}\ddot{\mathbf{U}}$$

2.2. A dispersion error analysis

Here we study the dispersion errors using the proposed explicit method and the central difference method when solving a two-dimensional wave propagation problem. For the spatial discretization, we consider a uniform mesh of 4-node elements.

Consider the solution of the scalar wave propagation governed by

$$\frac{\partial^2 u}{\partial t^2} - c_0^2\nabla^2 u = 0 \tag{24}$$

where u is the field variable and c_0 is the exact wave velocity. The corresponding finite element equations are [1]

$$\mathbf{M}\ddot{\mathbf{U}} + c_0^2\mathbf{K}\mathbf{U} = \mathbf{0} \tag{25}$$

where

$$\mathbf{M}^{(m)} = \frac{1}{4}\int_{V^{(m)}} dV^{(m)} \cdot \begin{bmatrix} 1 & 0 & 0 & 0 \\ 0 & 1 & 0 & 0 \\ 0 & 0 & 1 & 0 \\ 0 & 0 & 0 & 1 \end{bmatrix} \tag{26}$$

$$\mathbf{K}^{(m)} = \int_{V^{(m)}} (\nabla\mathbf{H}^{(m)})^T(\nabla\mathbf{H}^{(m)})dV^{(m)} \tag{27}$$

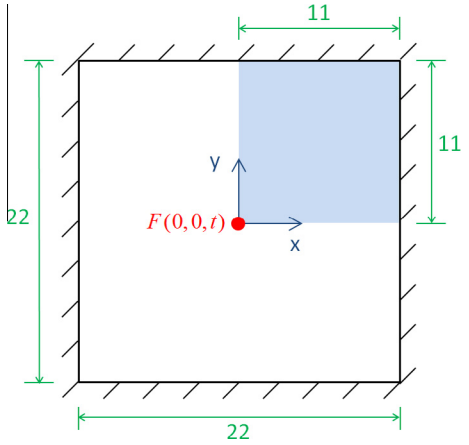

Fig. 8. Pre-stressed membrane problem, $c_0 = 1$, initial displacement and velocity are zero, computational domain is shaded.

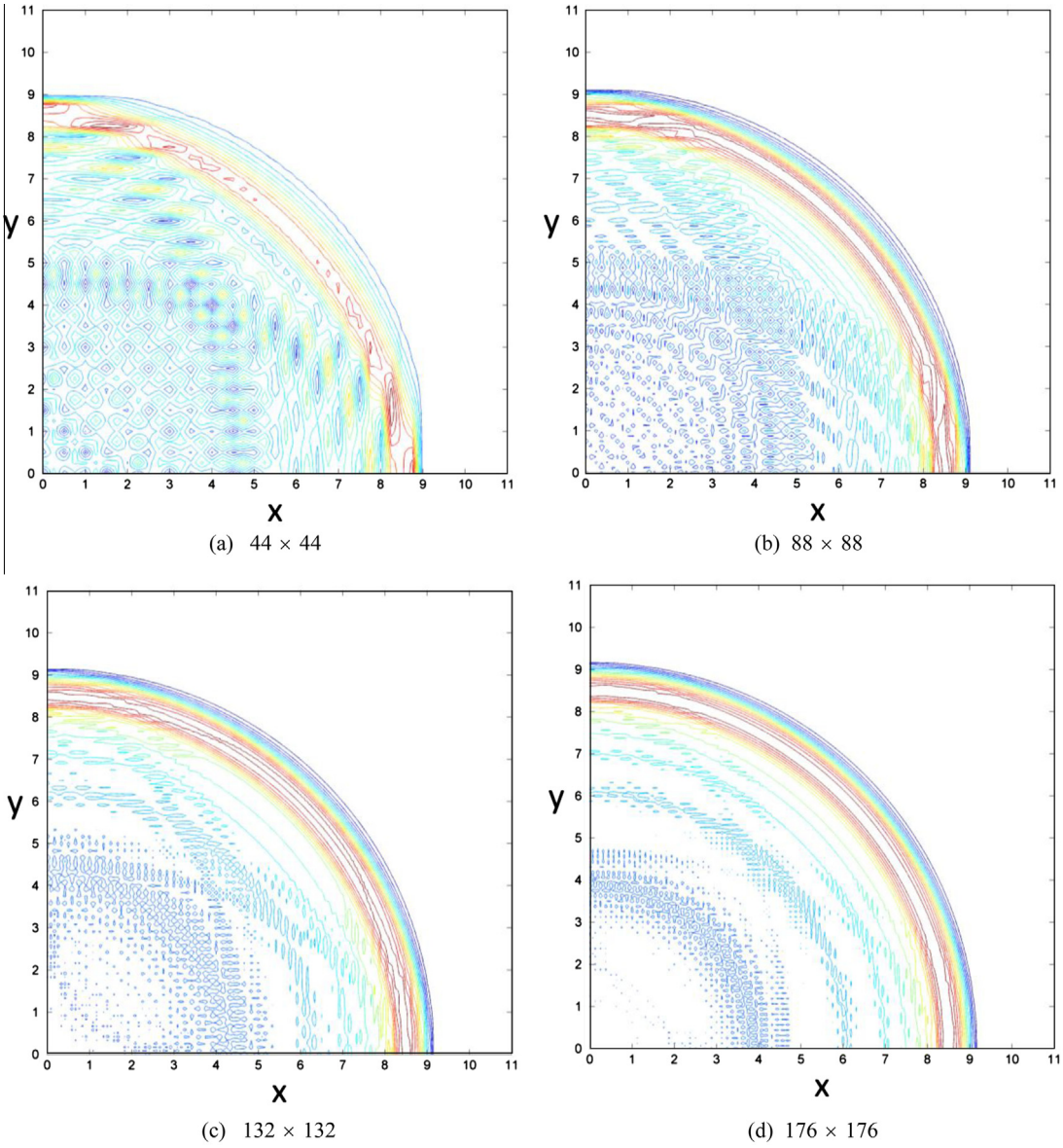

Fig. 9. Snapshots of displacements at $t = 9.25$, Central Difference method, CFL = 1.

and $\mathbf{H}^{(m)}$ and $\mathbf{U}$ are the element displacement interpolation matrix and the nodal displacement values of the solution, respectively, and $\mathbf{K}^{(m)}$ and $\mathbf{M}^{(m)}$ are the stiffness and lumped mass matrices for element (m) with volume $V^{(m)}$. In the actual evaluation, we use a unit thickness in accordance with Eq. (24).

Using Eqs. (13)–(15), we obtain a linear multistep form of the explicit scheme in the modal basis

$$^{t+\Delta t}x + (-2 + \Delta t^2\omega^2 + \alpha_1\Delta t^4\omega^4)\,^{t}x + (1 + \beta_1\Delta t^4\omega^4)\,^{t-\Delta t}x = 0 \quad (28)$$

or for all n equations [1]

$$^{t+\Delta t}\mathbf{X} + (-2\mathbf{I} + \Delta t^2\mathbf{\Lambda} + \alpha_1\Delta t^4\mathbf{\Lambda}^2)\,^{t}\mathbf{X} + (\mathbf{I} + \beta_1\Delta t^4\mathbf{\Lambda}^2)\,^{t-\Delta t}\mathbf{X} = \mathbf{0} \quad (29)$$

where

$$\alpha_1 = \frac{1}{2}p^2(p-1); \quad \beta_1 = -\frac{1}{2}p^3 + \frac{5}{4}p^2 - p + \frac{1}{4} \quad (30)$$

Here, x is a modal degree of freedom and $\mathbf{X}$ is the vector of all modal degrees of freedom, ω is the natural frequency of a generic mode of the finite element model and $\mathbf{\Lambda}$ is the corresponding diagonal matrix listing all ω_i^2.

Now using the eigenvectors $\mathbf{\Phi}$ of the problem

$$c_o^2\mathbf{K}\mathbf{\Phi} = \mathbf{M}\mathbf{\Phi}\mathbf{\Lambda} \quad (31)$$

and the definition $\mathrm{CFL} = \frac{c_0\Delta t}{h}$, where $h = \Delta x = \Delta y$, Eq. (29) can be written using the finite element degrees of freedom

$$^{t+\Delta t}\mathbf{U} + (-2\mathbf{I} + \mathrm{CFL}^2\mathbf{K} + \alpha_1\mathrm{CFL}^4\mathbf{K}^2)\,^{t}\mathbf{U} + (\mathbf{I} + \beta_1\mathrm{CFL}^4\mathbf{K}^2)\,^{t-\Delta t}\mathbf{U} = \mathbf{0} \quad (32)$$

For the central difference method [1], the governing equation is in the modal basis

$$^{t+\Delta t}x + (-2 + \Delta t^2\omega^2)\,^{t}x + {}^{t-\Delta t}x = 0 \quad (33)$$

and using the finite element degrees of freedom

$$^{t+\Delta t}\mathbf{U} + (-2\mathbf{I} + \mathrm{CFL}^2\mathbf{K})\,^{t}\mathbf{U} + {}^{t-\Delta t}\mathbf{U} = \mathbf{0} \quad (34)$$

Comparing Eqs. (32) and (34), the proposed explicit scheme contains additional terms proportional to $(\mathrm{CFL}^2\mathbf{K})^2$ that are multiplied by known displacement vectors (as required in an explicit scheme).

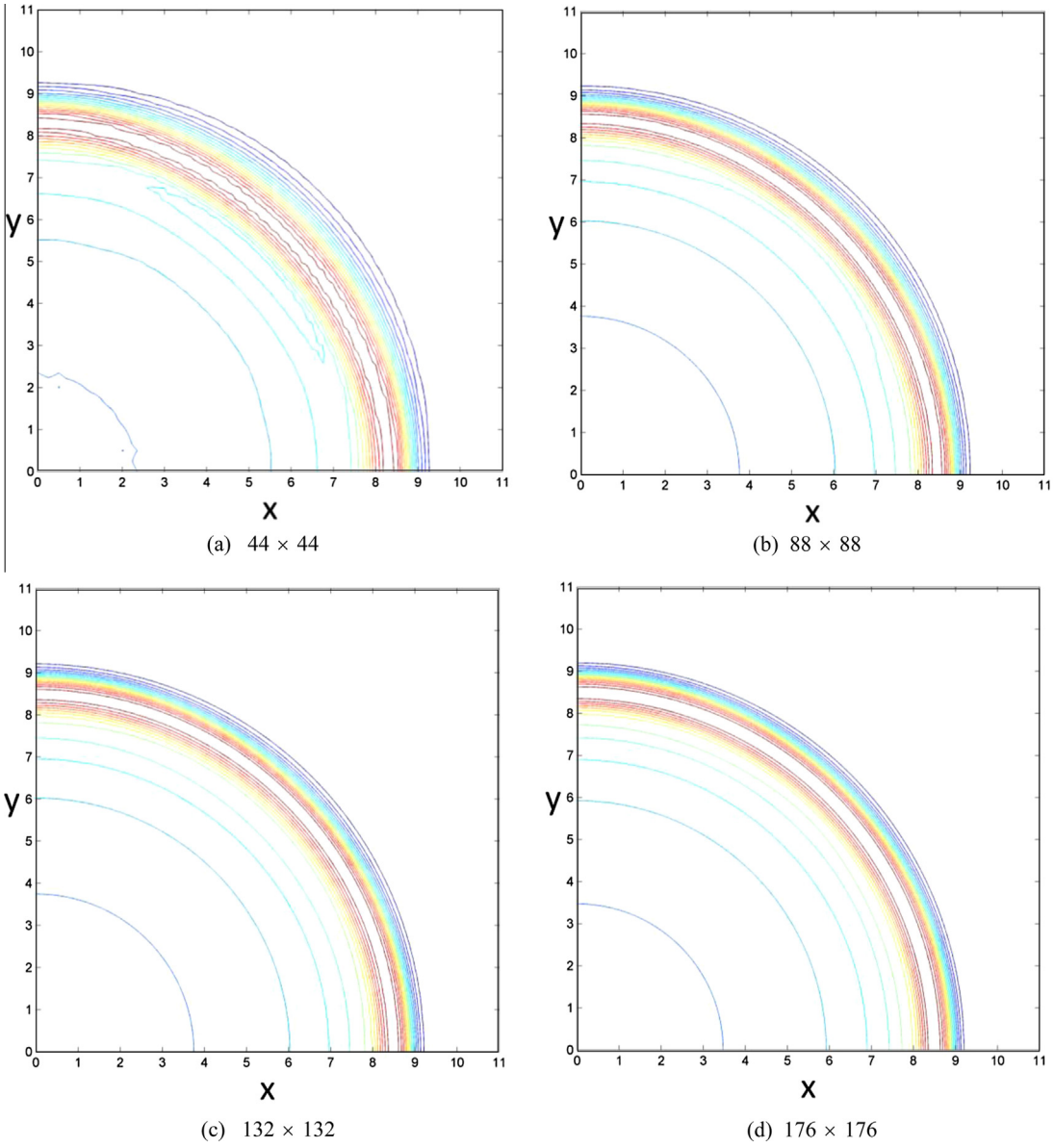

Fig. 10. Snapshots of displacements at $t = 9.25$, Proposed method, CFL = 1.85, $p = 0.54$.

In two-dimensional analyses, the general solution of Eq. (24) for a plane wave has the form $u = Ae^{i(k_0 x\cos(\theta)+k_0 y\sin(\theta)-\omega_0 t)}$, where ω_0 is the exact frequency of the wave mode and $k_0 = \omega_0/c_0$ is the corresponding exact wave number. The numerical solution takes the general form

$$ {}^{t}_{x,y}u = A_k e^{i(kx\cos(\theta)+ky\sin(\theta)-\omega t)} \tag{35}$$

where ω, $k = \omega/c$ and θ are, respectively, the numerical frequency, the corresponding wave number and the propagating angle measured from the x-axis. Numerical dispersion arises because the numerical wave speed c is different from the exact wave speed c_0 and a function of the wave number. In addition, the amplitude decay due to the time integration causes the decrease of the amplitude of the calculated wave.

For the uniform mesh, the solution of the finite element system at time $n_t\Delta t$ and location $n_x h$, $n_y h$ is

$$\begin{aligned} {}^{n_t\Delta t}_{n_x h,n_y h}u &= A_k e^{i(kn_x h\cos(\theta)+kn_y h\sin(\theta)-\omega n_t\Delta t)} \\ &= A_k e^{ikh(n_x\cos(\theta)+n_y\sin(\theta)-n_t(\mathrm{CFL})(c/c_0))} \end{aligned} \tag{36}$$

Substituting the above expression into Eqs. (32) and (34), the equation corresponding to the middle node of a patch of elements (16 finite elements for Eq. (32) and 4 finite elements for Eq. (34)) gives a relation between CFL = $c_0\Delta t/h$, c/c_0, the wave number k, and the element size h for the proposed method and the central difference method.

Note that the corresponding $\mathbf{K}^t\mathbf{U}$ term for the middle node at (x, y) is

$$\frac{1}{3}\left[8\,{}^{t}_{x,y}u - \left({}^{t}_{x\pm h,y}u + {}^{t}_{x,y\pm h}u + {}^{t}_{x\pm h,y\pm h}u\right)\right] \tag{37}$$

and the corresponding term from $\mathbf{K}^{2t}\mathbf{U}$ is

$$\begin{aligned} \frac{1}{9}\Big[72\,{}^{t}_{x,y}u - 12\left({}^{t}_{x\pm h,y}u + {}^{t}_{x,y\pm h}u\right) - 14\,{}^{t}_{x\pm h,y\pm h}u + 3\left({}^{t}_{x\pm 2h,y}u + {}^{t}_{x,y\pm 2h}u\right) \\ + 2\left({}^{t}_{x\pm 2h,y\pm h}u + {}^{t}_{x\pm h,y\pm 2h}u\right) + {}^{t}_{x\pm 2h,y\pm 2h}u\Big] \end{aligned} \tag{38}$$

To analyze the effect of the CFL number on the numerical dispersion, we first consider the case of zero propagating angle, $\theta = 0$. Figs. 4 and 5 show that as the CFL number increases, the dispersion

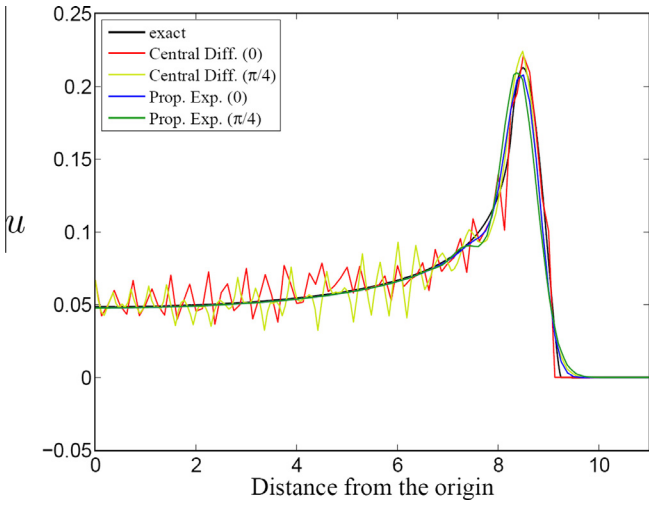

Fig. 11. Displacement variations along the various propagating angles, at time $t = 9.25$, 88×88 element mesh.

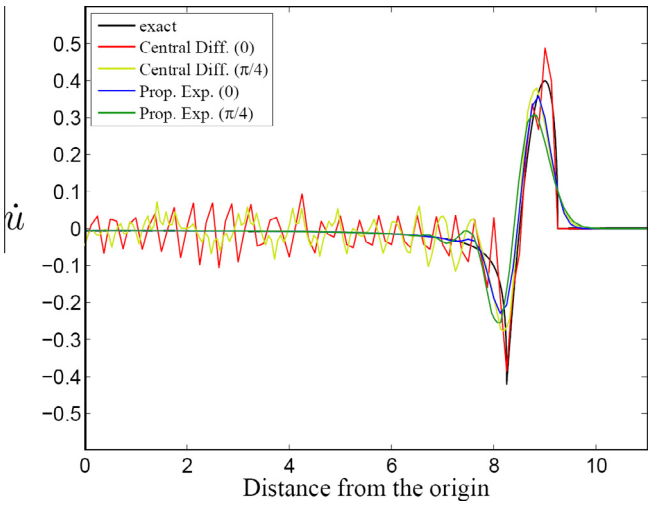

Fig. 12. Velocity variations along the various propagating angles, at time $t = 9.25$, 88×88 element mesh.

error gets smaller for both the proposed method and the central difference method. As well known, for CFL = 1, the central difference method provides no dispersion error.

For the proposed method, when using CFL = 1.85, the modes up to $k\Delta x \cong 1$ are accurately integrated with a small dispersion error (the maximum error is about 2%) and, what is important, the higher frequencies are cut out of the solution.

However, in actual practical analyses, waves will travel in all directions across elements, and it is important to have a small dispersion error for all propagating angles. Figs. 6 and 7 show the dispersion error curves for various propagating angles of the proposed method using CFL = 1.85 and the central difference method with CFL = 1. The dispersion errors in both methods increase as θ increases.

The important point is that the characteristics of the proposed method also hold for the multidimensional case. Due to cutting out higher frequencies, the overall dispersion error in the proposed scheme is quite small, while the errors in the central difference method can be large. Hence, solutions using the central difference method will generally show a significant dispersion error in 2D and 3D analyses.

It is interesting to note that the effect of increasing the propagation angle on the dispersion error curves in Figs. 6 and 7 is similar to those of decreasing the CFL number in Figs. 4 and 5. Hence, larger angles of propagation result in errors like using smaller CFL numbers. This is opposite to what is seen using an implicit method with the consistent mass matrix. The difference can be explained by the observation that we have period elongations in implicit methods and period shortenings in explicit methods. An important point is that, in the use of explicit time integration methods with the lumped mass matrix, larger angles of propagation have the same effect as using a smaller time step size for the time integration method. Therefore, if we set the time step size based on $\theta = 0$, then we satisfy the stability condition for all angles of wave propagations.

2.3. Selection of load magnitude at sub-step

Here, we study how the proposed time integration scheme interprets external forces defined at discrete time points. A typical modal equation of Eq. (25) is

$$\ddot{x} + \omega^2 x = r \tag{39}$$

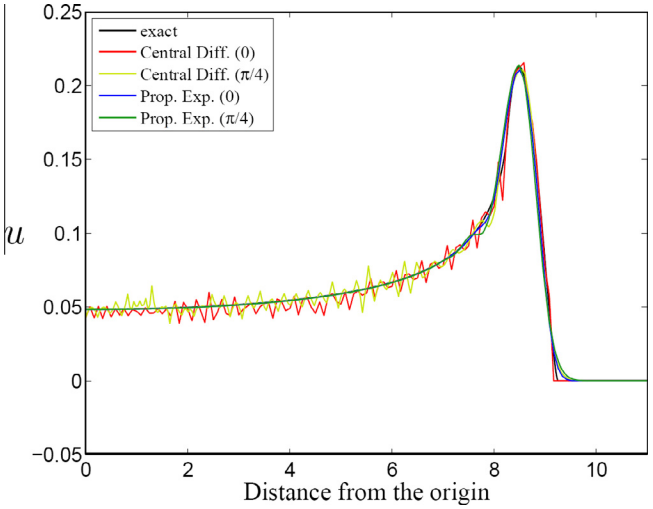

Fig. 13. Displacement variations along the various propagating angles, at time $t = 9.25$, 132×132 element mesh.

Considering the time domain from t_1 to t_2 we obtain

$$\int_{t_1}^{t_2} (r - \omega^2 x)dt = \int_{t_1}^{t_2} \ddot{x}dt \tag{40}$$

or

$$\int_{t_1}^{t_2} (r - \omega^2 x)dt = \int_{t_1}^{t_2} d\dot{x} \tag{41}$$

In the first sub-step, from t to $t + p\Delta t$, we use

$$\int_{t}^{t+p\Delta t} (r - \omega^2 x)dt = \frac{1}{2} p\Delta t({}^{t}\ddot{x} + {}^{t+p\Delta t}\ddot{x}) \tag{42}$$

where we applied Eqs. (4) and (5). Note that here the integral sign indicates the numerically approximated integration by the time integration scheme. Using the equilibrium equation, Eq. (39), at time points t and $t + p\Delta t$, and the fact that Eq. (40) holds for a general loading and trajectory, we obtain that the approximation used is

$$\int_{t}^{t+p\Delta t} r dt = \frac{1}{2} p\Delta t({}^{t}r + {}^{t+p\Delta t}\hat{r}) \tag{43}$$

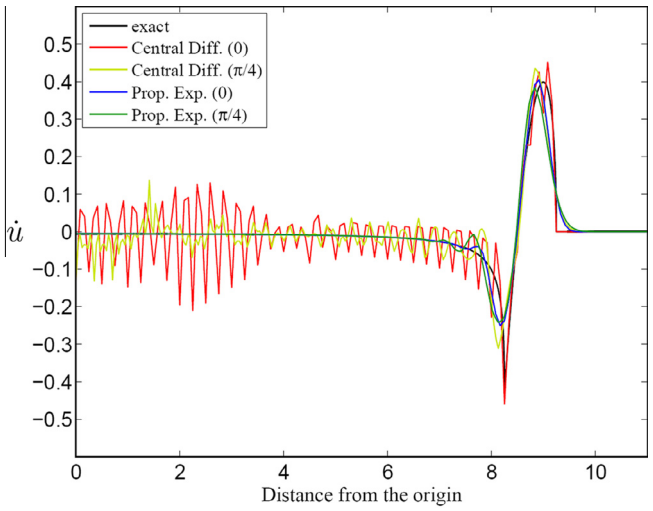

Fig. 14. Velocity variations along the various propagating angles, at time $t = 9.25$, 132×132 element mesh.

where ${}^{t+p\Delta t}\hat{r}$ is the modal load at time $t + p\Delta t$ corresponding to the load vector ${}^{t+p\Delta t}\widehat{\mathbf{R}}$ in Eq. (2).

Similarly, we obtain for the second sub-step

$$\int_{t+p\Delta t}^{t+\Delta t} r dt = (1-p)\Delta t\left(q_0\,{}^{t}r + \left(q_1 + \frac{1}{2}\right){}^{t+p\Delta t}\hat{r} + q_2\,{}^{t+\Delta t}r\right) \tag{44}$$

Hence, from Eqs. (43) and (44) and using the relations in Eqs. (12) and (21), the proposed scheme uses

$$\int_{t}^{t+\Delta t} r dt = \frac{\Delta t}{2}\left(\frac{-p^2+3p-1}{p}\,{}^{t}r + \frac{1-p}{p}\,{}^{t+p\Delta t}\hat{r} + p\,{}^{t+\Delta t}r\right) \tag{45}$$

In general, external loads are defined and sampled at discrete time points only, and these values are used for the external forces at the beginning and the end of each time step in direct time integration methods. If external loads are given at times t and $t + \Delta t$ as ^{t}r and ${}^{t+\Delta t}$r, then the best value in the sub-step to be used is

$${}^{t+p\Delta t}\hat{r} = (1-p)\,{}^{t}r + p\,{}^{t+\Delta t}r \tag{46}$$

which corresponds to the "mean" value and integrates the load by the trapezoidal rule over the time step. Of course, for smooth loads

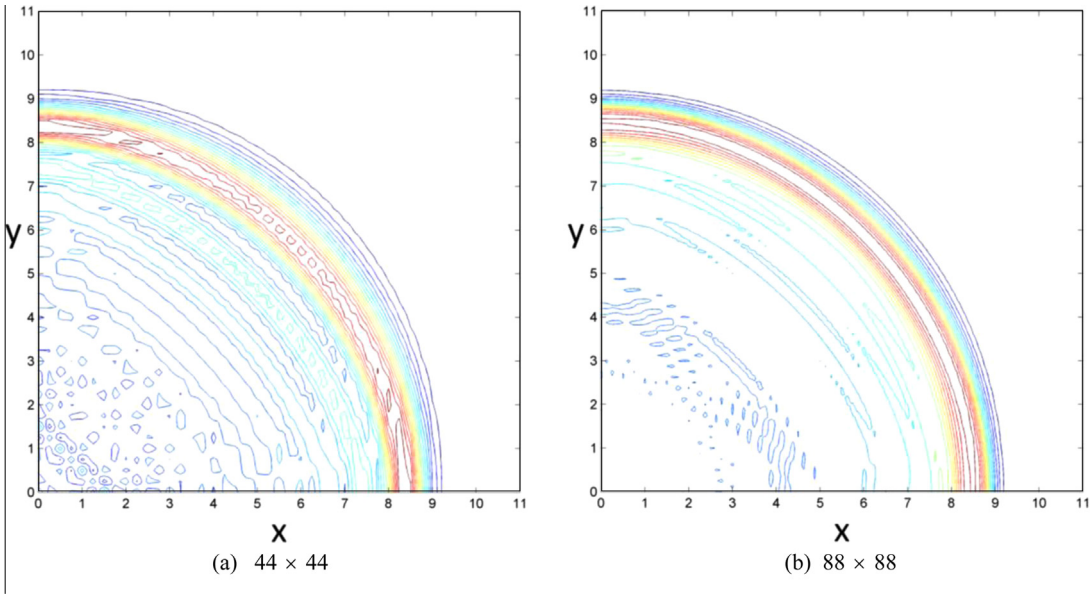

(a) 44×44 (b) 88×88

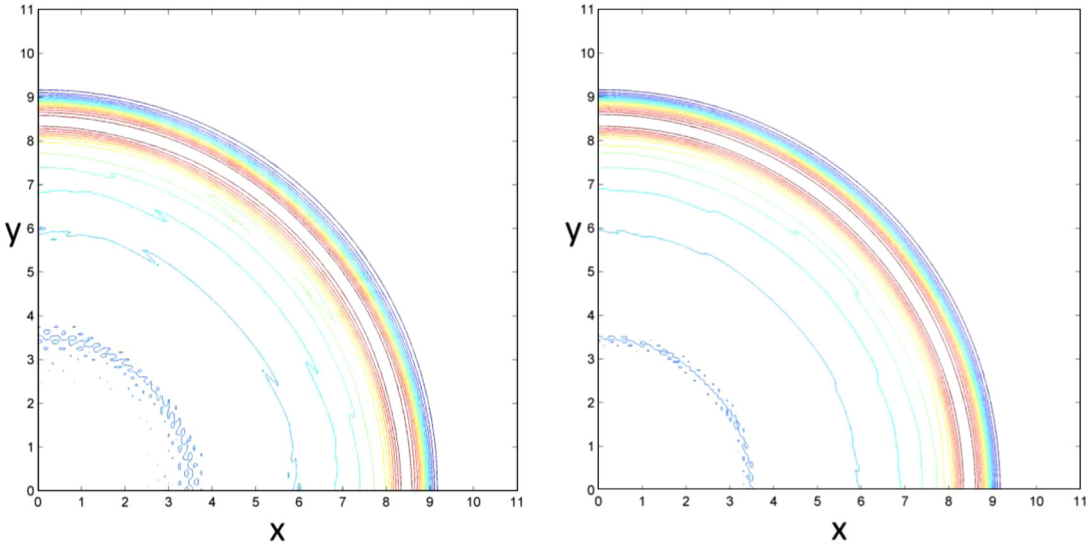

(c) 132×132 (d) 176×176

Fig. 15. Snapshots of displacements at $t = 9.225$, Tchamwa–Wielgosz scheme, $\varphi = 1.007$, CFL = 0.9.

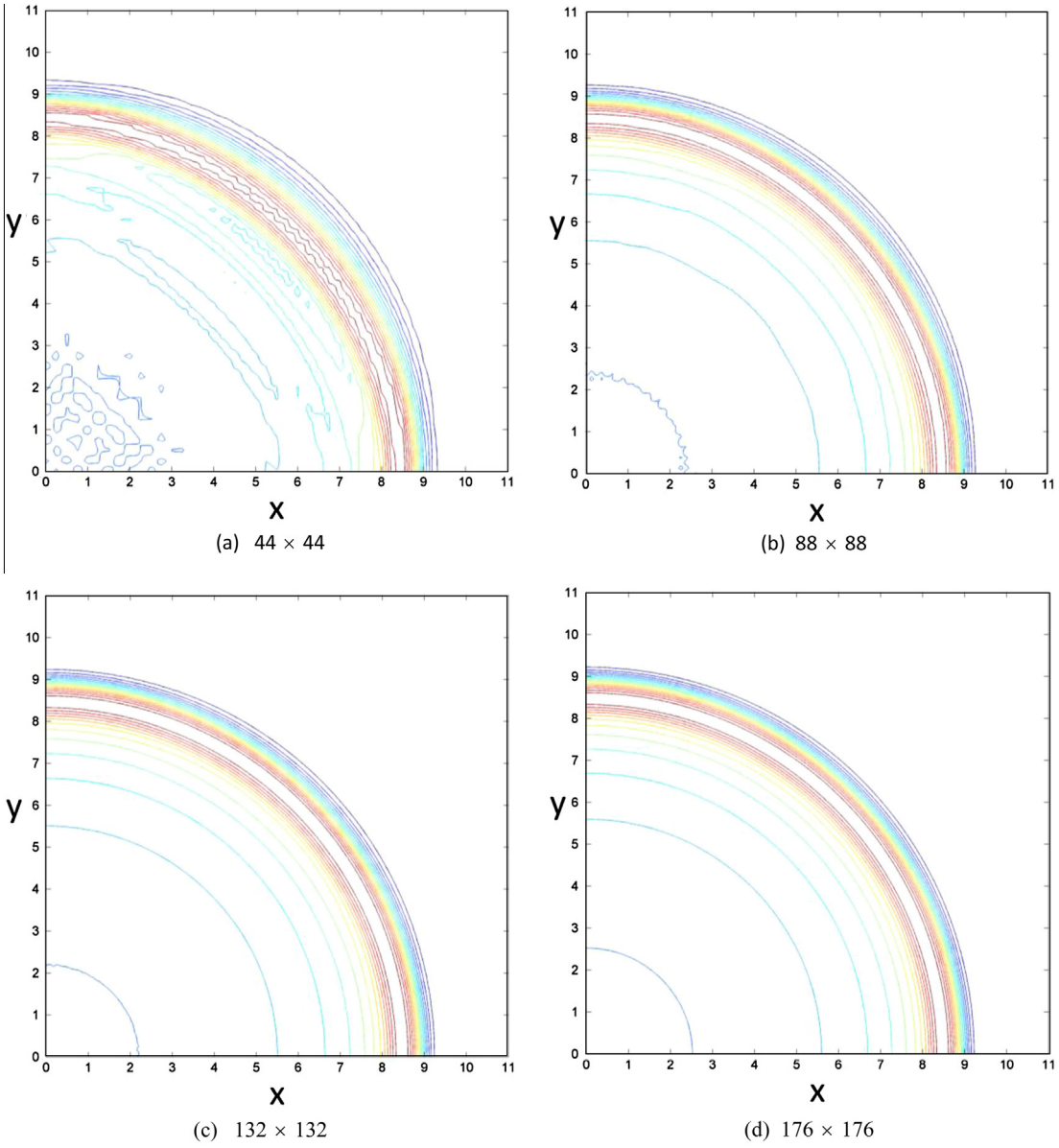

Fig. 16. Snapshots of displacements at $t = 9.225$, Tchamwa–Wielgosz scheme, $\varphi = 1.033$, CFL = 0.9.

also the actual value of the load at time $t + p\Delta t$ can be used. Note that a similar analysis for the Bathe implicit method shows that for rapidly varying loads also the "mean" value of the loads at times t and $t + \Delta t$ is best used.

The resulting procedure of the proposed explicit method for linear systems is summarized in Table 1. Comparing the number of operations needed per step when damping is neglected, we note that in using the proposed scheme, as for the central difference method, by far most computational expense is in evaluating the elastic nodal forces corresponding to given displacements. Hence, using the CFL number = 1.85 for the proposed scheme, the computational effort is near that of using the central difference method and the Tchamwa–Wielgosz scheme.

3. Wave propagation solutions

In this section, we present the solutions of some wave propagation problems using the proposed scheme. We first solve a 2D

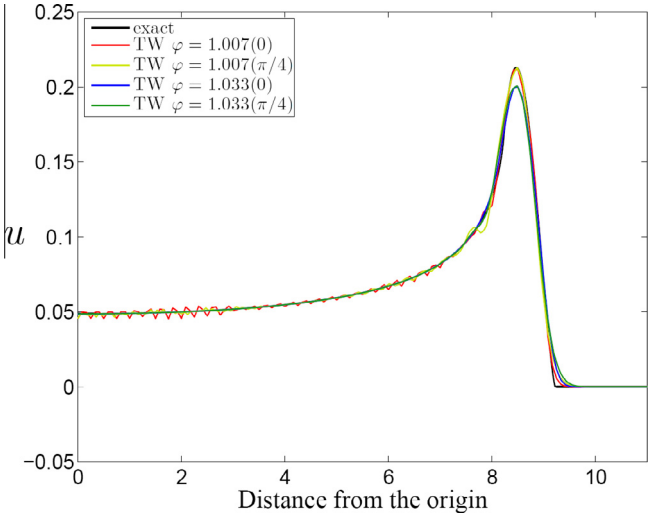

Fig. 17. Displacement variations along various propagating angles, at time $t = 9.225$, Tchamwa–Wielgosz scheme, 132 × 132 element mesh.

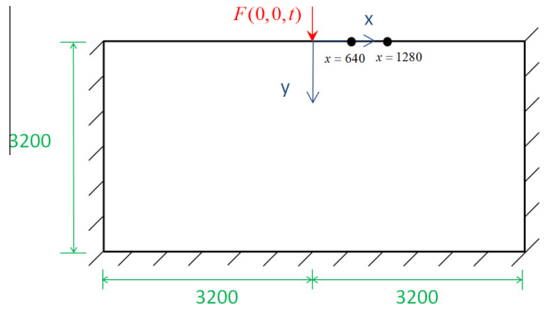

Fig. 18. A Lamb problem. $V_P = 3200$, $V_S = 1848$, $V_{Rayleigh} = 1671$; two receivers are placed at $x = 640$ and $x = 1280$; using symmetry only the right side of the domain is modeled.

transient scalar wave propagation and then a Lamb problem with two types of external loadings.

3.1. 2D scalar wave propagation

We consider a pre-stressed membrane, see Fig. 8, for which the governing equation is

$$\frac{\partial^2 u}{\partial x^2} + \frac{\partial^2 u}{\partial y^2} + F(0,0,t) = \frac{1}{c_0^2}\frac{\partial^2 u}{\partial t^2} \tag{47}$$

where u is the transverse displacement and c_0 is the wave velocity, here set to 1.0. The load is given as

$$F(0,0,t) = 4(1-(2t-1)^2)H(1-t), \quad t > 0 \tag{48}$$

where H is the unit step function. Due to symmetry, only the domain $[0,11] \times [0,11]$ is discretized and since the wave does not propagate to the boundary for the solution time considered, no absorbing boundary conditions are employed.

The proposed explicit method and the central difference method are used with the CFL numbers 1.85 and 1, respectively. For the CFL numbers, the length of the sides of the elements is used as the fundamental length; hence, the stability criteria are satisfied in each case.

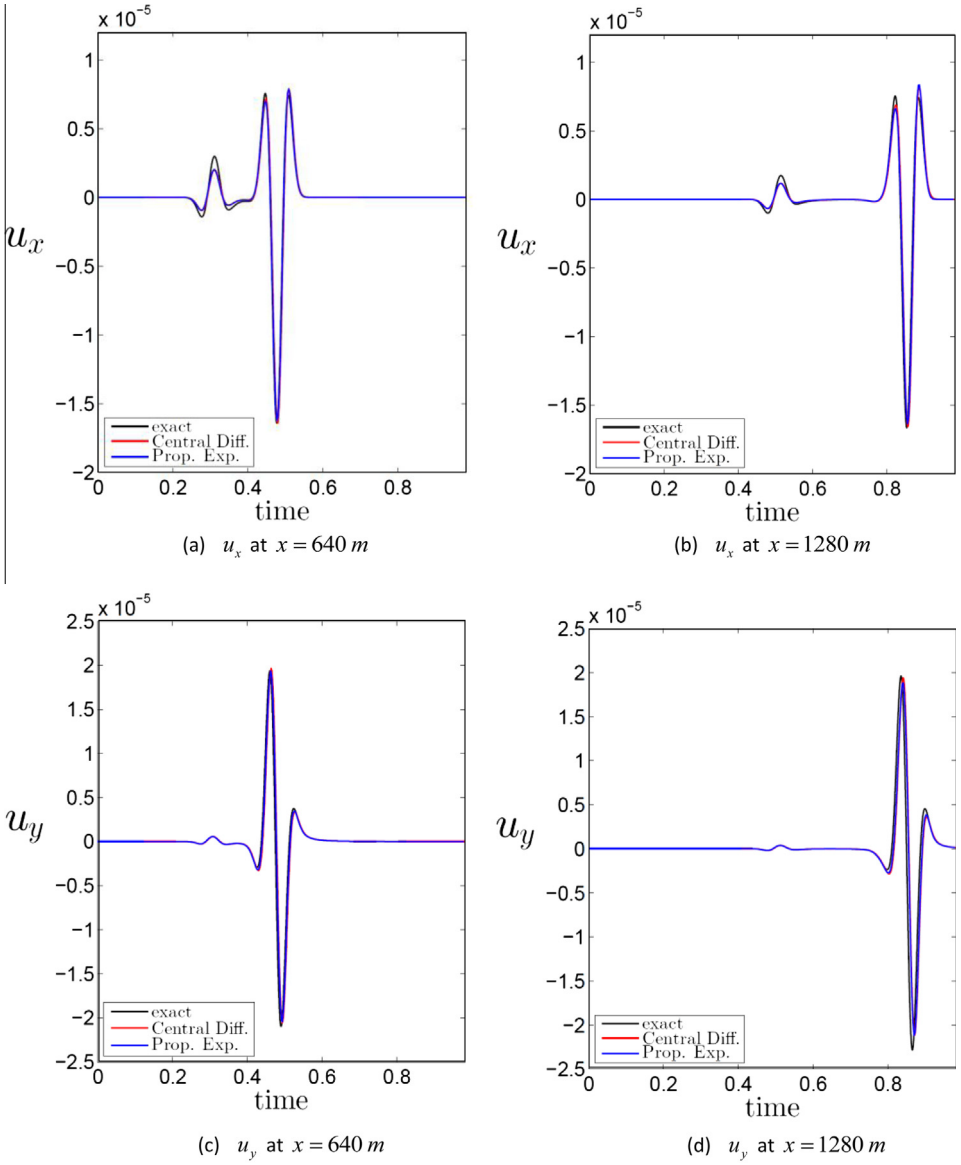

Fig. 19. Time history of displacement variations in x-direction and y-direction at the two receivers on the surface; Ricker wavelet line load.

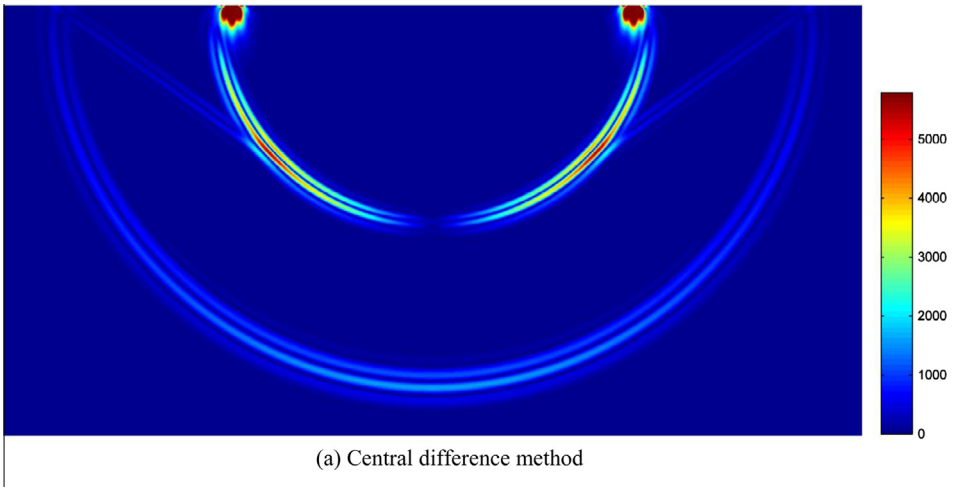

(a) Central difference method

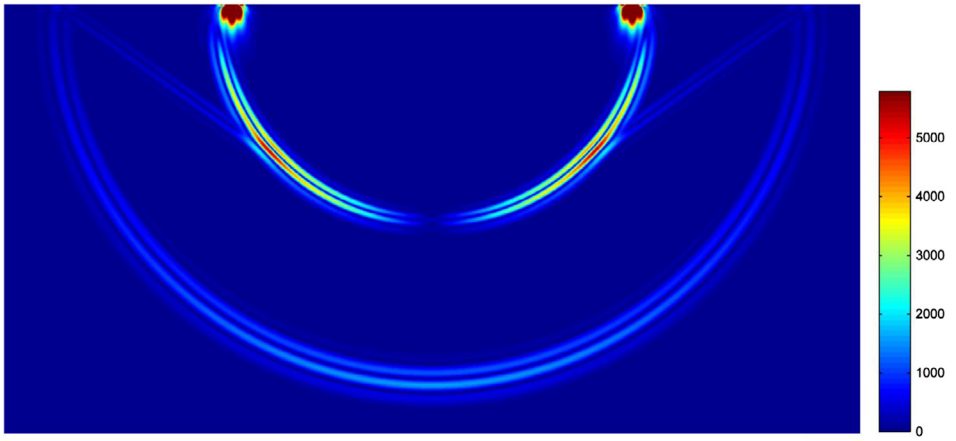

(b) Proposed explicit method

Fig. 20. Snapshots of von Mises stress at $t = 0.9828$ s; Ricker wavelet line load. (a) Central difference method. (b) Proposed explicit method.

Figs. 9 and 10 show snapshots of the solution variable u, calculated using the central difference method and the proposed scheme at $t = 9.25$ for various meshes. The results show that using a coarse mesh both methods give spurious oscillations. However, the proposed method provides a reasonably accurate solution using the 88×88 element mesh while the solution accuracy of the central difference method is still not good when using the 176×176 element mesh.

In Figs. 11–14, the numerical results at angles 0 and $\pi/4$ at time $t = 9.25$ using the 88×88 and 132×132 meshes are compared with the corresponding analytical solution. The central difference method gives noticeable spurious oscillations. The solution for u using the proposed method is reasonably accurate using either mesh, but considering the predicted velocity a significant solution error is seen in the peak value of $\dot{u}$ when using the 88×88 mesh. Also, larger solution errors for the response at the angle $\pi/4$ are observed, and these are well explained given Figs. 6 and 7.

To compare the predictive capabilities of the proposed method with those of the Tchamwa–Wielgosz scheme, we give in Figs. 15 and 16 snapshots of solutions using two values of φ and the CFL number = 0.9 as proposed in Ref. [37]. When $\varphi = 1.007$ is employed, spurious oscillations are still seen when using the mesh of 132×132 elements (and even still for the mesh of 176×176 elements). These oscillations are not present when $\varphi = 1.033$, but then the damping is rather large and the peak displacement is underestimated, see Fig. 17. Hence, it is crucial to use an appropriate value for φ in analyses, which may involve some numerical experimentation.

We observe that while the proposed method significantly improves the solution, the numerical solution of this example problem indicates that a high accuracy in the prediction of the velocity requires $\Delta x/(\lambda/2) \leqslant 0.2$. In fact, the proposed explicit method behaves quite similar to the Bathe implicit method, while the central difference method behaves similar to the trapezoidal rule [6].

3.2. Wave propagations in a semi-infinite elastic domain

We now consider a Lamb problem, in which waves are propagating in a semi-infinite elastic domain in plane strain conditions as described in Fig. 18. Here, the P-wave velocity = 3200 m/s, S-wave velocity = 1848 m/s, and the Rayleigh wave velocity = 1671 m/s. The time duration for computing the waves is 0.999 s, so that the P-wave does not reach the outer boundaries; hence no absorbing boundary conditions are employed.

For the time step size, we use the CFL numbers 1.85 and 1 for the proposed explicit method and the central difference method, respectively. For the CFL numbers, the length of the sides of the elements is used as the fundamental length, and the fastest wave, the P-wave, is used.

We consider first a Ricker wavelet line force defined as

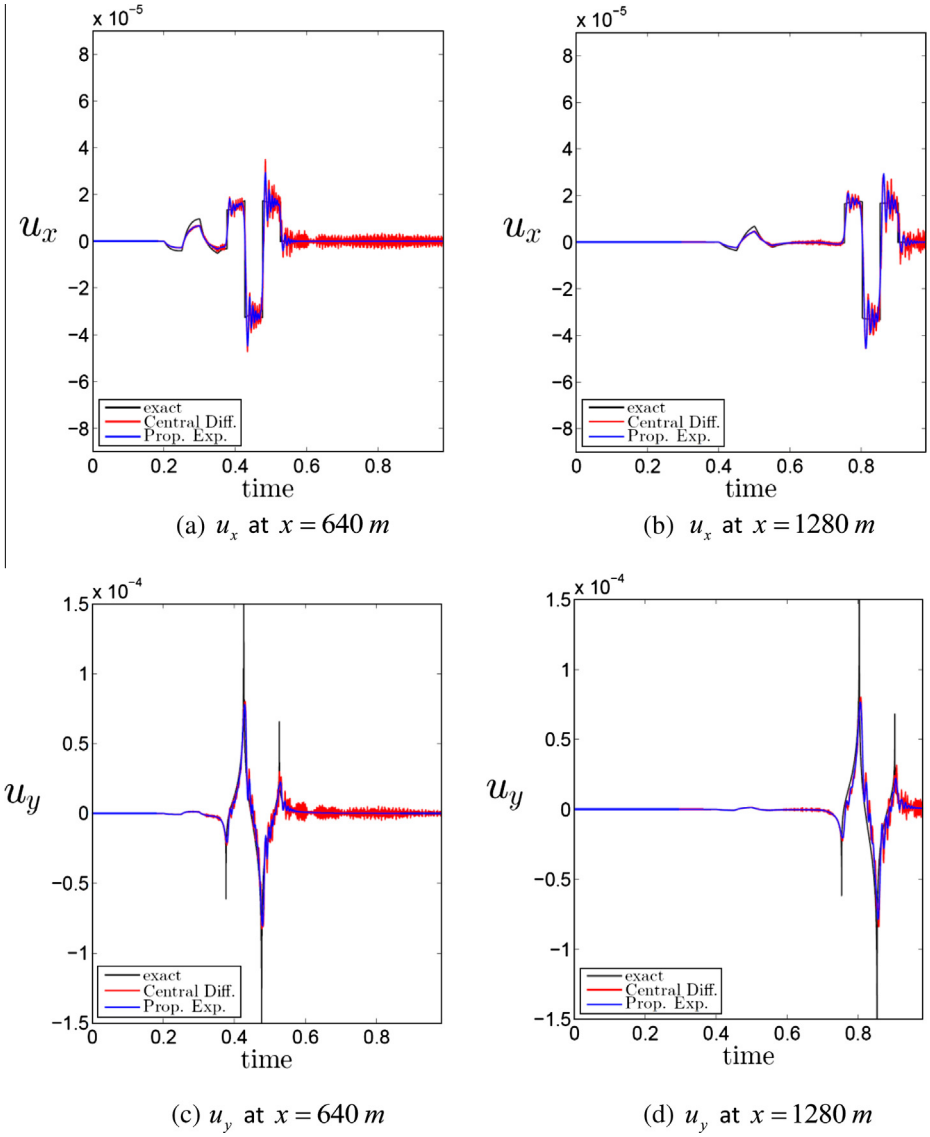

Fig. 21. Time history of displacement variations in x-direction and y-direction at the two receivers on the surface; line load of step functions.

$$F(0,0,t) = -10^6 \times (1 - 2\pi^2\hat{f}^2(t-t_0)^2)\exp(-\pi^2\hat{f}^2(t-t_0)^2), \quad t > 0 \tag{49}$$

with the frequency $\hat{f} = 12.5$ Hz and $t_0 = 0.1$ s. Using symmetry, only the right side of the domain in Fig. 18 is meshed using 640×640 4-node elements of side lengths $\Delta x = \Delta y = 5$ m. The calculated displacements are measured at $x = 640$ m and $x = 1280$ m from the source and the results are shown in Fig. 19. The analytical solution and the numerical solutions using, both, the proposed method and the central difference method are in good agreement.

The applied external load can be well approximated with only a few harmonic functions; therefore, a limited number of wave modes are excited. Hence, if a fine mesh is employed so that all excited wave modes are within $\Delta x/(\lambda/2) \leqslant 0.2$, as done here, both, the proposed explicit method and the central difference method provide very accurate solutions. The calculated von Mises stress at time $t = 0.9828$ using both methods is shown in Fig. 20.

We next consider the line force defined as

$$F(0,0,t) = 10^6 \times [H(0.15-t) - 3H(0.1-t) + 3H(0.05-t)], \quad t > 0 \tag{50}$$

Since the applied line load consists of three step functions, many wave modes are excited which renders the problem more difficult to solve. The computational domain is now meshed with 1600×1600 4-node elements of side lengths $\Delta x = \Delta y = 2$ m. Fig. 21 shows the displacements at the two receivers. While the solutions using both time integration methods show spurious oscillations, the predicted response using the proposed method is significantly more accurate.

We can see the difference in the solution accuracy more clearly when considering the predicted stress wave fields, as shown in Fig. 22. The predicted stress waves using the proposed method are quite sharp but the solution using the central difference method shows in various areas undesirable spurious oscillations.

4. Concluding remarks

We proposed a new explicit time integration method for the analysis of wave propagation problems. The scheme has been formulated using a sub-step within a time step to achieve desired numerical damping to suppress undesirable spurious oscillations of high frequencies but, in its final form, does not use an adjustable

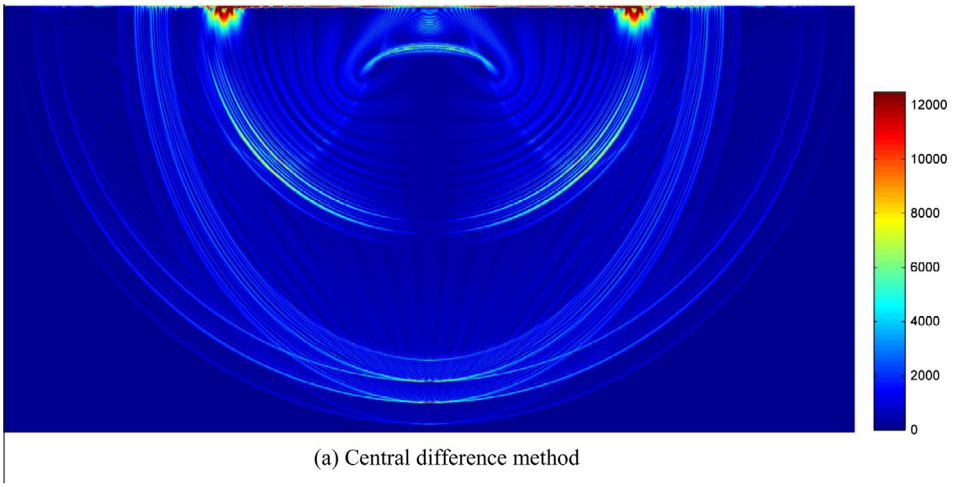

(a) Central difference method

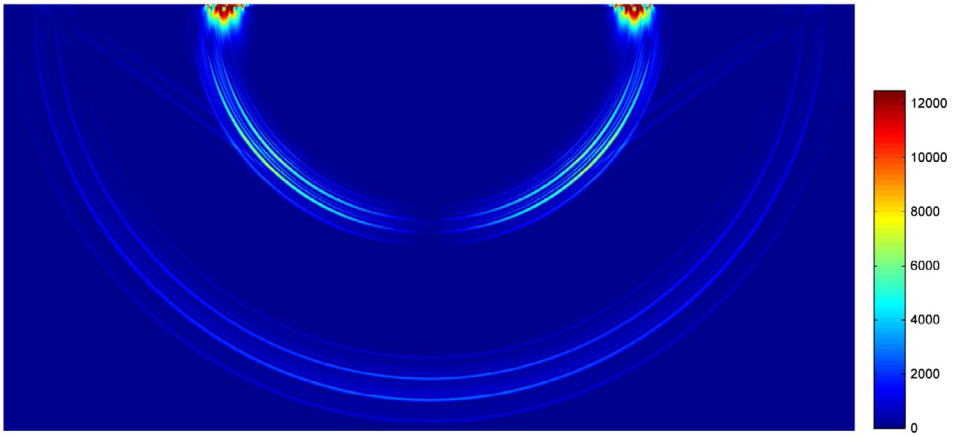

(b) Proposed explicit method

Fig. 22. Snapshots of von Mises stress at $t = 0.9828$ s; line load of step functions. (a) Central difference method. (b) Proposed explicit method.

parameter. The load at the sub-step is chosen for good accuracy. With the optimal CFL number $= 1/p \cong 1.85$ when $p = 0.54$, the method uses about 10% more solution effort as the standard central difference scheme but significantly improves the solution accuracy and a non-diagonal damping matrix can directly be included.

We discussed the stability and accuracy of the proposed scheme and presented the performance in the solution of some wave propagation problems. As in the Bathe implicit method, we observed that the wave modes that cannot be spatially represented are cut out of the calculated response [6]. Of course, the scheme can also be used for structural dynamics solutions although then frequently an implicit time integration method is more effective.

As mentioned in Section 1, there are a number of other explicit schemes available that also provide numerical damping in the solution. While we have given some comparisons regarding the properties of the proposed scheme and the Tchamwa–Wielgosz method, a further comparison and evaluation including also other techniques by, for example, solving a suite of benchmark problems would be valuable.

To solve a wave propagation problem, a good spatial discretization is also important. In this paper we only considered the linear element in uniform meshes to focus on the basic characteristics of the time integration scheme. Theoretical and numerical studies of the behaviour of the proposed method when using higher-order element discretizations, distorted meshes and enriched finite element schemes, like given in Ref. [15], would valuable.

Appendix A. The integration operator A and load operators $\mathbf{L_a}$ and $\mathbf{L_b}$

Using the relations in Eqs. (12) and (21), we obtain the expressions for the integration operator **A** and load operators $\mathbf{L_a}$ and $\mathbf{L_b}$:

$$\mathbf{A} = \begin{bmatrix} a_{11} & a_{12} & a_{13} \\ a_{21} & a_{22} & a_{23} \\ a_{31} & a_{32} & a_{33} \end{bmatrix} \tag{51}$$

$$\mathbf{L_a} = \begin{bmatrix} \frac{1}{2}(p-1)\Omega_0^2 + \xi(-2+p)\Omega_0 \\ \frac{\Delta t}{2p}((1+\Omega_0((1/2)\Omega_0+\xi)p^3 - 2\Omega_0((1/4)\Omega_0+\xi)p^2 - p)) \\ -\frac{\Delta t^2}{2}(p-1) \end{bmatrix} \tag{52}$$

$$\mathbf{L_b} = \begin{bmatrix} 1 \\ \frac{p\Delta t}{2} \\ 0 \end{bmatrix} \tag{53}$$

where

$$a_{11} = -\frac{p\Omega_0}{2}((-(1/2)p + (1/2)p^2)\Omega_0^3 + \xi(p^2-2)\Omega_0^2 + (1 + (-8+4p)\xi^2)\Omega_0 + 2\xi) \quad (54)$$

$$a_{12} = -\frac{\Omega_0}{\Delta t}\left((-(1/2)p + (1/2)p^2)\Omega_0^3 + \xi(-1+p^2-p)\Omega_0^2 + (1 + (-4+2p)\xi^2)\Omega_0 + 2\xi\right) \quad (55)$$

$$a_{13} = -\frac{\Omega_0^2}{\Delta t^2}\left(1 + ((1/2)p - (1/2))\Omega_0^2 + \xi(-2+p)\Omega_0\right) \quad (56)$$

$$a_{21} = -\frac{\Delta t}{8p}\begin{pmatrix} p^5\Omega_0^4 + 2p^5\xi\Omega_0^3 - p^4\Omega_0^4 + 8p^4\xi^2\Omega_0^2 - 4\xi\Omega_0^3p^3 \\ +4p^3\xi\Omega_0 - 16p^3\xi^2\Omega_0^2 - 8\xi\Omega_0p^2 + 4p^2 + 2\Omega_0^2p^2 \\ +8\xi\Omega_0p - 12p + 4 \end{pmatrix} \quad (57)$$

$$a_{22} = \frac{1}{4p}\begin{pmatrix} (-p^4+p^3)\Omega_0^4 - 2\xi p^2(-1+p^2-p)\Omega_0^3 \\ +(8\xi^2p^2 - 4p^3\xi^2 - 2p)\Omega_0^2 - 4\xi(-p+p^2+1)\Omega_0 + 4p \end{pmatrix} \quad (58)$$

$$a_{23} = -\frac{\Omega_0^2}{2p\Delta t}\left(1 + \Omega_0((1/2)\Omega_0 + \xi)p^3 + \left(1 - (1/2)\Omega_0^2 - 2\xi\Omega_0\right)p^2 - p\right) \quad (59)$$

$$a_{31} = \frac{1}{4}\left(2 + (p^2-p)\Omega_0^2 + 4\xi(p-1)\Omega_0\right)\Delta t^2 p \quad (60)$$

$$a_{32} = \frac{\Delta t}{2}\left(2 + (p^2-p)\Omega_0^2 + 2\xi(p-1)\Omega_0\right) \quad (61)$$

$$a_{33} = 1 + \frac{1}{2}(p-1)\Omega_0^2 \quad (62)$$

References

[1] Bathe KJ. Finite element procedures. Prentice Hall; 1996.
[2] Wood WL. Practical time-stepping schemes. Oxford: Claredon Press; 1990.
[3] Chung J, Lee JM. A new family of explicit time integration methods for linear and non-linear structural dynamics. Int J Numer Methods Eng 1994;37:3961–76.
[4] Hulbert GM, Chung J. Explicit time integration algorithms for structural dynamics with optimal numerical dissipation. Comput Methods Appl Mech Eng 1996;137:175–88.
[5] Chang SY, Liao WI. An unconditionally stable explicit method for structural dynamics. J Earthqauke Eng 2005;9:349–70.
[6] Noh G, Ham S, Bathe KJ. Performance of an implicit time integration scheme in the analysis of wave propagations. Comput Struct 2013;123:93–105.
[7] Chin RCY. Dispersion and Gibbs phenomenon associated with difference approximations to initial boundary-value problems for hyperbolic equations. J Comput Phys 1975;18:233–47.
[8] Babuska IM, Sauter SA. Is the pollution effect of the FEM avoidable for the Helmholtz equation considering high wave numbers? SIAM Rev 2000;42:451–84.
[9] Bao G, Wei GW, Zhao S. Numerical solution of the Helmholtz equation with high wave numbers. Int J Numer Methods Eng 2004;59:389–408.
[10] Payen DJ, Bathe KJ. A stress improvement procedure. Comput Struct 2012;112–113:311–26.
[11] Gottlieb D, Orszag SA. Numerical analysis of spectral methods: theory and applications. Capital City Press; 1993.
[12] Karniadakis GE, Sherwin SJ. Spectral/hp element methods for computational fluid dynamics. Oxford University Press; 2005.
[13] Gamallo P, Astley RJ. The partition of unity finite element method for short wave acoustic propagation on non-uniform potential flows. Int J Numer Methods Eng 2006;65:425–44.
[14] Kohno H, Bathe KJ, Wright JC. A finite element procedure for multiscale wave equations with application to plasma waves. Comput Struct 2010;88:87–94.
[15] Ham S, Bathe KJ. A finite element method enriched for wave propagation problems. Comput Struct 2012;94–95:1–12.
[16] Kim J, Bathe KJ. The finite element method enriched by interpolation covers. Comput Struct 2013;116:35–49.
[17] Mullen R, Belytschko T. Dispersion analysis of finite element semidiscretizations of the two-dimensional wave equation. Int J Numer Methods Eng 1982;18:11–29.
[18] Marfurt KJ. Accuracy of finite-difference and finite-element modeling of the scalar and elastic wave-equations. Geophysics 1984;49:533–49.
[19] Christon MA. influence of the mass matrix on the dispersive nature of the semi-discrete, second-order wave equation. Comput Methods Appl Mech Eng 1999;173:147–66.
[20] Krenk S. Dispersion-corrected explicit integration of the wave equation. Comput Method Appl Mech Eng 2001;191:975–87.
[21] Seriani G, Oliveira SP. Optimal blended spectral-element operators for acoustic wave modeling. Geophysics 2007;72:95–106.
[22] Guddati MN, Yue B. Modified integration rules for reducing dispersion error in finite element methods. Comput Method Appl Mech Eng 2004;193:275–87.
[23] Yue B, Guddati MN. Dispersion-reducing finite elements for transient acoustics. J Acoust Soc Am 2005;118:2132–41.
[24] Idesman AV, Schmidt M, Foley JR. Accurate finite element modeling of linear elastodynamics problems with the reduced dispersion error. Comput Mech 2011;47:555–72.
[25] Holmes N, Belytschko T. Postprocessing of finite element transient response calculations by digital filters. Comput Struct 1976;6:211–6.
[26] Idesman A, Samajder H, Aulisa E, Seshaiyer P. Benchmark problems for wave propagation in elastic materials. Comput Mech 2009;43:797–814.
[27] Kuhl D, Crisfield MA. Energy-conserving and decaying algorithms in non-linear structural dynamics. Int J Numer Methods Eng 1999;45:569–99.
[28] Fung TC. Numerical dissipation in time-step integration algorithms for structural dynamic analysis. Prog Struct Eng Mater 2003;5:167–80.
[29] Bathe KJ, Baig MMI. On a composite implicit time integration procedure for nonlinear dynamics. Comput Struct 2005;83:2513–24.
[30] Bathe KJ. Conserving energy and momentum in nonlinear dynamics: a simple implicit time integration scheme. Comput Struct 2007;85:437–45.
[31] Bathe KJ, Noh G. Insight into an implicit time integration scheme for structural dynamics. Comput Struct 2012;98–99:1–6.
[32] Kazanci Z, Bathe KJ. Crushing and crashing of tubes with implicit time integration. Int J Impact Eng 2012;42:80–8.
[33] Dahlquist G. A special stability problem for linear multistep methods. BIT 1963;3:27–43.
[34] Krieg RD. Unconditional stability in numerical time integration methods. J Appl Math 1973;40:417–21.
[35] Warburton GB. Some recent advances in structural vibration. In: Brebbia IA, Orszag SA, editors. Vibrations of engineering structures. Lecture notes in engineering, vol. 10. Berlin: Springer; 1963. p. 215–24.
[36] Hahn GD. A modified Euler method for dynamic analyses. Int J Numer Methods Eng 1991;32:943–55.
[37] Maheo L, Grolleau V, Rio G. Numerical damping of spurious oscillations: a comparison between the bulk viscosity methods and the explicit dissipative Tchamwa–Wielgosz scheme. Comput Mech 2013;51:109–28.
[38] Newmark N. A method of computation for structural dynamics. J Eng Mech Div ASCE 1959;85:67–94.
[39] Zhai WM. Two simple fast integration methods for large scale dynamic problems in engineering. Int J Numer Methods Eng 1996;39:4199–214.
[40] Tchamwa B, Conway T, Wielgosz C. An accurate explicit direct time integration method for computational structural dynamics. In: Kwon YW, Chung HH, editors. Recent advances in solids and structures, vol. 398. ASME-PUBLICATIONS-PVP; 1999. p. 77–84.
[41] Rio G, Soive A, Grolleau V. Comparative study of numerical explicit time integration algorithms. Adv Eng Softw 2005;35:252–65.
[42] Nsiampa N, Ponthot J, Noels L. Comparative study of numerical explicit schemes for impact problems. Int J Impact Eng 2008;35:1688–94.
[43] Wilson EL, Farhoomand I, Bathe KJ. Nonlinear dynamic analysis of complex structures. Earthquake Eng Struct 1973;1:241–52.
[44] Bathe KJ, Wilson EL. Stability and accuracy analysis of direct integration methods. Earthquake Eng Struct 1973;1:283–91.
[45] Bathe KJ. On reliable finite element methods for extreme loading conditions. In: Ibrahimbegovic A, Kozar I, editors. Chapter in extreme man-made and natural hazards in dynamics of structures. Springer; 2007.